Turkish Journal of Electrical Engineering & Computer Sciences

http://journals.tubitak.gov.tr/elektrik/

Research Article

Turk J Elec Eng & Comp Sci
(2015) 23: 1025 – 1039
© TÜBİTAK
doi:10.3906/elk-1303-118

Superior decoupled control of active and reactive power for three-phase voltage source converters

Hesam RAHBARIMAGHAM, Erfan MAALI AMIRI, Behrooz VAHIDI*, Gevorg BABAMALEK GHAREHPETIAN, Mehrdad ABEDI
Department of Electrical Engineering, Amirkabir University of Technology, Tehran, Iran

Received: 18.03.2013 • **Accepted/Published Online:** 02.07.2013 • **Printed:** 10.06.2015

Abstract: This paper presents an active-reactive power control strategy for voltage source converters (VSCs) based on derivation of the direct and quadrature components of the VSC output current. The proposed method utilizes a multivariable proportional-integral controller and provides almost completely decoupled control capability of the active and reactive power with almost full disturbance rejection due to step changes in the power exchanged between the VSC and the grid. It also imposes fast transient response and zero steady-state error as compared to the conventional power control approaches. The applicability of the proposed power control strategy for providing the robust stability of the system against the uncertainties of the load parameters is also investigated. The superiority of the proposed control strategy over conventional approaches in the new condition of supplying the load is demonstrated. The theoretical aspects of the proposed multivariable-based power control strategy and the conventional approaches are reviewed and simulation results are presented in two separate sections. MATLAB/Simulink 2009a is used to simulate different scenarios of the simulation.

Key words: Unified power flow controller, equivalent impedance modeling, optimization, voltage index

1. Introduction

Utilizing renewable energies such as distributed generation (DG) has become a great concern for utility grids to provide sufficient electrical energy to supply domestic and industrial requirements in a clean world. There are many types of these generations, including wind energy [1–5] and photovoltaic and fuel cells [6–9]. Many of these technologies adopt voltage source converters (VSCs) as an interface of distributed generators because of the nature of the output voltage. VSCs give us advantages including easy controllability and the capability to control circuit parameters like the voltage, current, or output power of the DG [10–15]. There are three types of control strategies adopted for the VSCs: 1) active-reactive power control (called PQ control), 2) active power-voltage control (PV control), and 3) voltage-frequency control (VF control).

Many approaches utilized proportional-integral (PI)-based controllers to regulate the target variable at the desired level. PI controllers are universally known because of their simple implementation and tuning and for providing fast dynamics and zero steady-state error [16]. These controllers are always used for various applications of current regulation [17–23]. Regulating a variable in a rotating reference frame (RRF) is defined when time-varying variables (AC variables) are transferred to an orthogonal space like the *dq0* domain, in which the frame rotates with an arbitrary angular speed of ω. This makes the variables appear as time-invariant

*Correspondence: vahidi@aut.ac.ir

quantities. Therefore, the designed controller can act like a DC/DC converter with zero steady-state error by providing an infinite gain at the operating point. In these methods, the controller should have the capability of decoupling the dq axis components of one variable such that the unwanted disturbances applied to one axis do not generate significant transients on the other one. This capability provides independent control of the desired variable, which could be the output current or the power of a converter.

In [24], a multivariable PI-based dq current control strategy based on a different design procedure than the conventional approaches [25] was proposed to reach the desired decoupling between the two d and q axis components of the line current. The presented method provides much less transient effect against incoming disturbances and zero steady-state error on tracking the reference values; moreover, it has a simple structure and is easy to implement. However, in the utility grids, due to changes in the demanded power imposed by the loads, what is important is that the distributed generators with power electronic interface could supply the requested power. This could be possible by applying the appropriate methods. The decoupling capability between the two d and q axis components of the current is also applicable for the active and reactive power exchanged between the VSC and grid. In [26], a classical droop control method was utilized to achieve the grid impedance. The virtual real and reactive power frame transformation was then used to result in decoupling power control capability. Wei and Kao [27] proposed a power control strategy based on placing a virtual inductance at the inverter output in a low-voltage microgrid. The impedance voltage droop and the local load effects were considered to prevent the coupling between the active and reactive output power, but one of the problems of the conventional droop control method is the assumption that the output impedance is mainly inductive. To avoid using extra output inductance, fast control loops were added to the droop method [28]. In [29], a control scheme was utilized that used the voltage and current variation at the point of common coupling due to small changes of the VSI power for estimating the grid impedance so that power flow control could be possible in all conditions of the grid including on-grid or autonomous mode.

In this paper, the application of a multivariable PI-controller in the power control strategy for VSC-based DG has been presented. In the proposed method, first the reference values of direct and quadrature components of the converter output current are determined directly from specified power references. Because these values are proportional to the active and reactive output power, respectively, a controller is then utilized to regulate the output power at the desired level. The capability of the designed controller has been shown from various points of view: 1) improvement of the transient response, 2) zero steady-state error in tracking the power reference values, 3) capability of minimizing the effect of step changing in output active or reactive power on one another for decoupling control capability of these powers, and 4) robust stability of the controller against uncertainties of load parameters. MATLAB/Simulink 2009a has been used to simulate the different scenarios of the simulation.

2. System description and modeling

A single-line diagram of the three-phase test system adopted for evaluating the performance of the proposed method is shown in Figure 1. In this system, a distributed generation unit is connected to the grid through a VSC interface module, with a series line reactor as a filter to reduce the harmonics generated due to the VSC and finally a coupling transformer to reach the grid voltage level. The DC side voltage of the VSC considered is constant like a battery. The internal resistance and inductance of the filter are considered as R_t and L_t, respectively. The inductance of the coupling transformer is latent in the filter inductance. The numerical values of the test system elements are given in the Table.

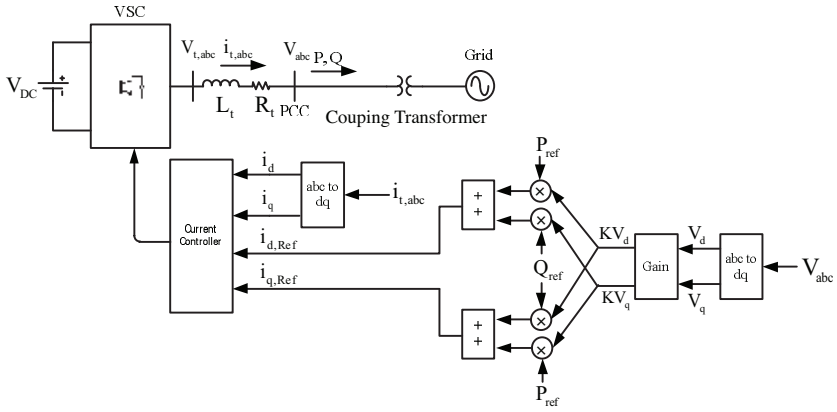

Figure 1. One-line diagram of the test system.

Table. Numerical values of the three-phase test system.

Component	Value	Comment
L_t	4.5 mH	Inductance of the VSC filter
R_t	0.1Ω	Resistance of the VSC filter
V_{dc}	450 V	DC bus voltage
V_s	380 V	Grid nominal line to line voltage
n_1:n_2	4:1	Transformer ratio
$S_{nominal,VSC}$	800 VAR	VSC rated power
f_{sw}	10 kHz	PWM carrier frequency
f_s	5 kHz	Sampling frequency
f	50 Hz	System nominal frequency

2.1. Mathematical model of the test system

In this section, the mathematical model of the three-phase test system and its structure diagram is derived [30]. Based on Figure 1, which shows the structure of the test system, writing the KVL from the PCC bus to the converter terminal results in the dynamic equation of the VSC in the *abc* frame as below:

$$V_{t,abc} = R_t i_{t,abc} + L_t \frac{di_{t,abc}}{dt} + V_{abc}. \tag{1}$$

To design an applicable PI-based current controller in the rotating reference frame, Eq. (1), which is the dynamic representation of the system in the stationary rotating frame, should transform to the *dq* reference frame that rotates by the angular speed of ω. This transform could be done by the following expression:

$$F_{dq0} = K_S F_{abc}. \tag{2}$$

Eq. (2) transforms any *abc* quantities into the rotating frame, where K_s is defined as below:

$$K_S = \frac{2}{3}\begin{bmatrix} \cos\omega t & \cos(\omega t - 120) & \cos(\omega t + 120) \\ \sin\omega t & \sin(\omega t - 120) & \sin(\omega t + 120) \\ 1/2 & 1/2 & 1/2 \end{bmatrix}. \tag{3}$$

Therefore, the dynamic equation of the system in the RRF could result as in Eq. (4), in which the zero sequence has been neglected.

$$V_{t,dq} = R_t i_{t,dq} + L_t \frac{di_{t,dq}}{dt} + j\omega L_t i_{t,dq} + V_{dq} \tag{4}$$

The real and imaginary parts of Eq. (4) could be separated to achieve the dynamic equation of the system on the d and q direct axis in the RRF, such as in Eqs. (5) and (6). The block diagram of the test system is obtained in the dq frame by adopting Eqs. (5) and (6) and it is shown in Figure 2.

$$R_t i_{t,d} + L_t \frac{di_{t,d}}{dt} = V_{t,d} + \omega L_t i_{t,q} - V_d \tag{5}$$

$$R_t i_{t,q} + L_t \frac{di_{t,q}}{dt} = V_{t,q} - \omega L_t i_{t,d} - V_q \tag{6}$$

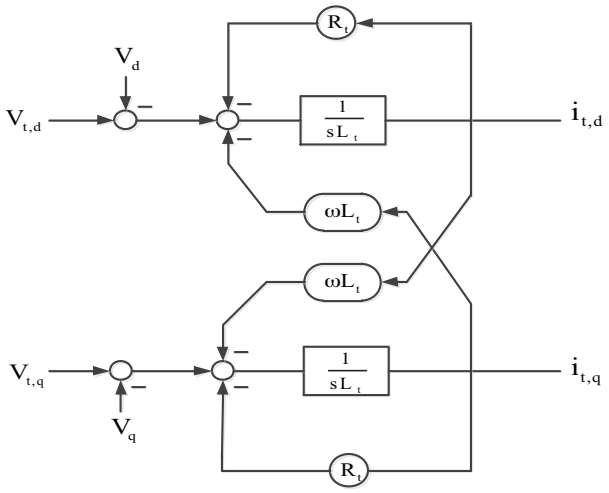

Figure 2. Structure diagram of the test system model [30].

3. Proposed PQ control strategy

One of the main goals of all power control strategies is avoiding the coupling between active and reactive power to fulfill an individual power control. The main structure of the conventional power control schemes is shown in Figure 3.

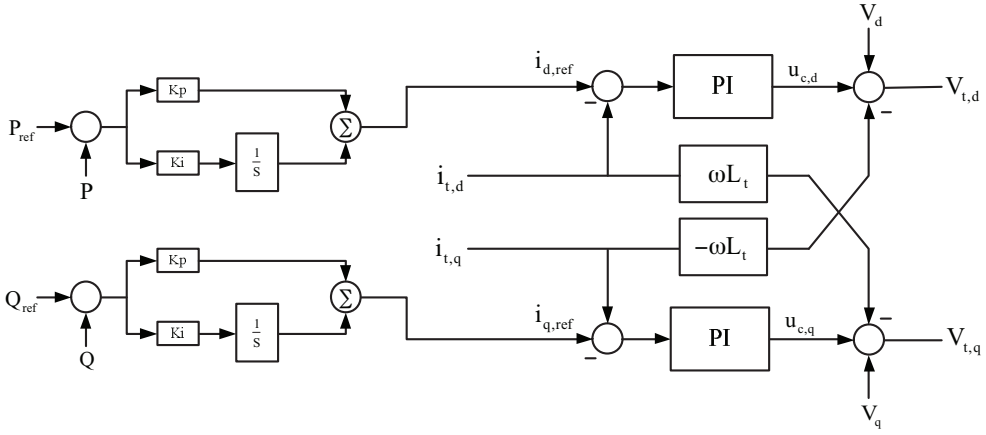

Figure 3. Structure diagram of the conventional power control scheme.

As is clear, in this structure the references of the d and q axis components of the VSC AC side current are obtained through two PI controllers by comparing the real and reference values of the active and reactive output power.

In this paper, the PQ control strategy proposed for fixing the active and reactive power of the VSC at the desired level is based on directly extracting the reference values of the VSC output current on the dq direct axis from the active and reactive power references without utilizing any PI controllers. The proposed method reduces the number of required controllers from four to two by removing the first stage of the structure, as shown in Figure 3. The second stage of Figure 3, which depicts the inner current control loop, was surveyed by two current control schemes to investigate the performance of each scheme. Considering the d and q components of the VSC output voltage and current, the instantaneous active and reactive output power could be represented as:

$$P_s(t) = \frac{3}{2}(V_{sd}(t)i_d(t) + V_{sq}(t)i_q(t)), \tag{7}$$

$$Q_s(t) = \frac{3}{2}(-V_{sd}(t)i_q(t) + V_{sq}(t)i_d(t)), \tag{8}$$

where V_{sd} and V_{sq} are the dq direct axis components of the output AC voltage and are fixed by the grid. Therefore, they cannot be controlled by the controller.

The dq components of the output current are obtained by considering the matrix inverse of Eq. (9), which is the matrix representing Eqs. (7) and (8):

$$\begin{bmatrix} i_d(t) \\ i_q(t) \end{bmatrix} = \frac{2}{3}\begin{bmatrix} V_{sd}(t) & V_{sq}(t) \\ V_{sq}(t) & -V_{sd}(t) \end{bmatrix}^{-1}\begin{bmatrix} P_s(t) \\ Q_s(t) \end{bmatrix}. \tag{9}$$

Substituting P_s and Q_s equal to P_{ref} and Q_{ref} respectively in (9), the dq current references are achieved as follows:

$$I_{d-ref} = \frac{2}{3}(\frac{V_d(t)}{V_d^2(t) + V_q^2(t)} \times P_{ref}(t) + \frac{V_q(t)}{V_d^2(t) + V_q^2(t)} \times Q_{ref}(t)), \tag{10}$$

$$I_{q-ref} = \frac{2}{3}(\frac{V_q(t)}{V_d^2(t) + V_q^2(t)} \times P_{ref}(t) - \frac{V_d(t)}{V_d^2(t) + V_q^2(t)} \times Q_{ref}(t)). \tag{11}$$

The obtained dq axis references are then applied to the current controllers to achieve the desired level of output power, such that the sudden variation in the active or reactive power demanded by utility appearing as step changes does not have a significant effect on the other one and possible controls on the active and reactive output power can be done independently. Figure 4 depicts the structural diagram of the proposed power control method. The outer control loop demonstrated with a dashed line has been changed and the PI controllers have been neglected.

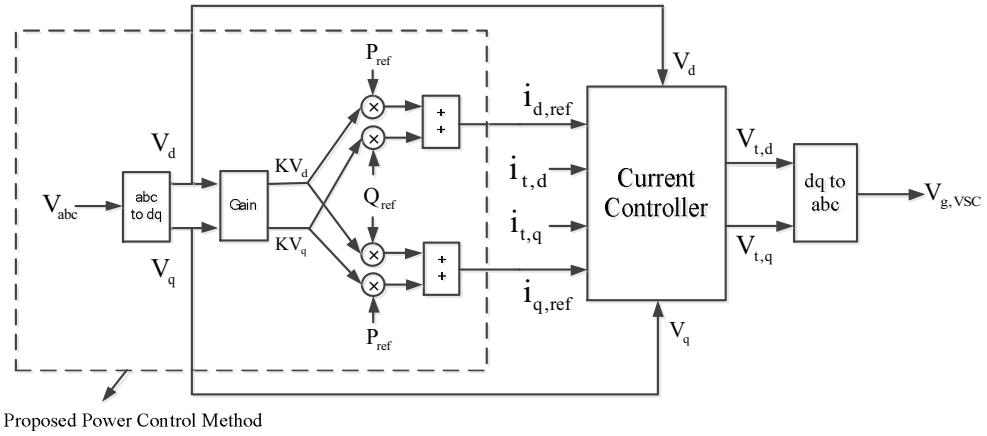

Figure 4. Structure diagram of the proposed power control scheme.

The proposed PQ control strategy can adopt various types of inner current control loop. Two kinds of current control strategies have been utilized as the inner loop and they are compared in the next sections to achieve better control of the output power of the VSC. This decoupled power control strategy is suitable for small-sized DG to manage the output power and reach the maximum power point tracking, especially in microgrids.

4. Controller design

This section investigates the application of two conventional and multivariable PI-based controllers [24] for regulating the output power. The design procedure of each controller and the manner of utilizing these approaches in power control strategy are described individually.

4.1. PQ control strategy based on conventional PI-controller

In this section, the conventional PI-based current controller as the inner loop has been designed considering the mathematical model derived in the previous section. The main structure of the conventional controller has been reviewed in many studies based on Eqs. (12) and (13). These equations illustrate how the dq components of the terminal voltage should be controlled [31].

$$v_{t,d} = u_{c,d} - L_t \omega i_{t,q} + v_d \tag{12}$$

$$v_{t,q} = u_{c,q} + L_t \omega i_{t,d} + v_q \tag{13}$$

Here, $u_{c,d}$ and $u_{c,q}$ are the output signals of the PI-controller, which are utilized as the control signals. Adopting Eqs. (12) and (13) in Eq. (4), the control signals could be obtained as follows:

$$u_{c,d} = L_t \frac{di_{t,d}}{dt} + R_t i_{t,d}, \tag{14}$$

$$u_{c,q} = L_t \frac{di_{t,q}}{dt} + R_t i_{t,q}. \tag{15}$$

Thus, the transfer function of the system to reach the d or q axis component of the line current could be acquired by Eqs. (14) and (15) as below:

$$G_s(s) = \frac{K_s}{1 + sT_s}, \tag{16}$$

where $T_s = L_t/R_t$ is the time constant and gain K_S is equal to $1/R_t$. The $i_{t,d}$ and $i_{t,q}$ values obtained by Eq. (16) in the previous step are regulated at the desired level by a PI-controller as $G_R(s)$ and then the control signals $u_{c,d}$ and $u_{c,q}$ are obtained and adopted to achieve the dq components of the terminal voltage. Therefore, the control of the terminal voltage according to Eqs. (12) and (13) is implemented by defining the feedforward and feedback signals from the dq components of the current and the PCC voltage, respectively. Figure 5 shows the structure of the proposed power control strategy that adopted the conventional current controller based on Eqs. (12) and (13).

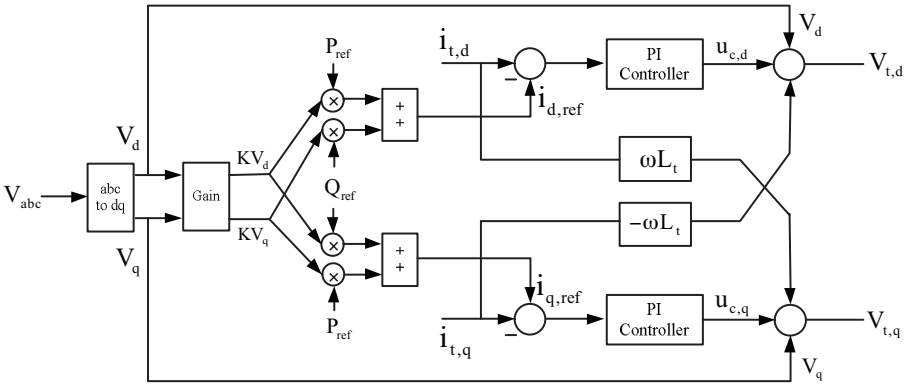

Figure 5. Block diagram of the power control strategy based on conventional current controller.

The effect of the pulse width modulation and the sampling and measurement time delays has been considered as a simple first-order transfer function, $G_{PE}(s)$ [32]. Incorporating all these transfer functions, the open-loop transfer function of the decoupled system can be represented by multiplying the transfer functions $G_R(s)$, $G_{PE}(s)$, and $G_s(s)$, as follows:

$$G_o(s) = G_R(s)\frac{K_{cm}}{1+sT_{PE}}\frac{K_s}{1+sT_s}. \tag{17}$$

The transfer function of the PI-controller is chosen such that after a zero-pole cancellation, the $G_o(s)$ could be simplified as:

$$G_o(s) = \frac{K}{sT_i(1+sT_{PE})}, \tag{18}$$

where T_i is the integration time constant determined by considering the phase margin for the system transfer function $G_o(s)$. By adopting the feedforward signals as shown in Figure 5, the effect of the coupling terms $\omega L_t i_d$ and $\omega L_t i_q$ is canceled theoretically. Therefore, according to Eqs. (10) and (11), which show the dependency of active and reactive power to i_d and i_q, it could be inferred that these powers could be controlled independently by adopting the current control loop as an inner loop after obtaining the current references from the specified power references. Therefore, the power control could be considered to be decoupled too, and then the decoupled system has been deduced. However, due to uncertainty of the circuit parameter values and measurement errors, it is practically not possible to have a fully decoupled system.

4.2. PQ control strategy based on multivariable PI-controller

Contrary to the introduced conventional PI-controller that utilized the feedforward signals to minimize the coupling between two axes, in designing the multivariable current controller the plant inversion technique has been used and is described as follows.

If Eq. (4) is the dynamic representation of the system in the RRF considered in Laplace domain, since the PCC voltage has been kept constant by the utility, the dq components of the $V(s)$ can be applied as negative feedforward signals to cancel its effect. Thus, the transfer function of the system according to Eq. (4) is deduced as:

$$G_s(s) = \frac{V_t - V}{I_t} = \frac{K_s}{1 + (s + j\omega)T_s}, \tag{19}$$

where T_s and K_s are the same parameters mentioned in Eq. (16). The term $j\omega T_s$ causes a coupling between two axes in the dq frame. Therefore, the open-loop transfer function of the system is obtained such as in Eq. (17) by adopting the above transfer function of the system.

$$G_o(s) = G_R(s)\frac{K_{cm}}{1 + sT_{PE}}\frac{K_s}{1 + (s + j\omega)T_s} \tag{20}$$

$G_R(s)$, the transfer function of the PI-controller, is chosen such that after a zero-pole cancellation between $G_R(s)$ and $G_s(s)$, the coupling term $j\omega T_s$ is removed. Thus, the transfer function of the PI-controller is chosen as follows:

$$G_R(s) = \frac{1 + (s + j\omega)T_n}{sT_i}, \tag{21}$$

where the time constants T_n and T_s are considered to be equal. Therefore, the final expression of the system's open-loop transfer function is simplified as:

$$G_o(s) = \frac{K}{sT_i(1 + sT_{PE})}, \tag{22}$$

where T_i is the integration time constant and K is equal to $K_{cm}K_s$. Absence of the $j\omega$ term in Eq. (22) causes the desired decoupling between the dq axes. To implement the structural diagram of the multivariable PI-controller utilized in the system and achieve the control signals in each direct axis, Eq. (21) is decomposed to real and imaginary parts as derived in Eqs. (23) and (24). Therefore, the block diagram of the proposed power control strategy designated based on the multivariable PI-controller could be depicted as in Figure 6. It can be concluded that because the integrators have been applied on the coupling terms, the effect of the two axes on each other is significantly reduced compared to the conventional approach.

$$u_{c,d} = \frac{1 + sT_n}{sT_i}i_{\varepsilon,d} - \frac{\omega T_n}{sT_i}i_{\varepsilon,q} \tag{23}$$

$$u_{c,q} = \frac{1 + sT_n}{sT_i}i_{\varepsilon,q} + \frac{\omega T_n}{sT_i}i_{\varepsilon,d} \tag{24}$$

5. Simulation results

In this section, the performance of the two proposed controllers is evaluated from three points of view: 1) decoupling capability between active and reactive power exchanged between the VSC and grid; 2) tracking of the references signals of two kinds of power, which is determined by the utility, and the references signals of dq current components, which are produced by the proposed method in Section 3, 3) and fast dynamics and transient response. Each control strategy has been tested when sudden stepping up/down changes happen in one power reference value while another is kept constant. First the conventional case is investigated.

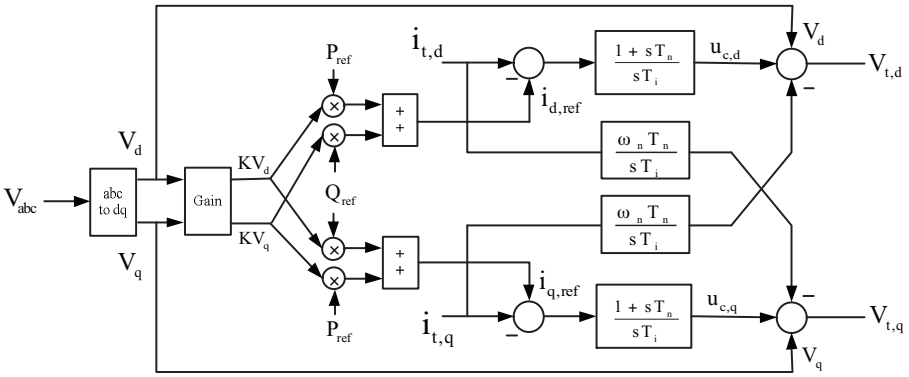

Figure 6. Block diagram of the power control strategy based on multivariable current controller.

Both the active and reactive power injected by the converter into the grid are assumed to be 0.8 p.u. At t = 0.3 s the active power value changes to –0.7 p.u. and at t = 0.35 s it steps back to the previous value. In the whole of this interval, the reactive power value is kept constant. Figures 7a and 7b illustrate the changes in the reference of the active power while the reactive power is constant, also depicting that, due to the step changes in active power, the reactive power experiences a significant transient. Therefore, in this control strategy, two kinds of power are not fully decoupled from each other. Figures 7c and 7d show the variation of the reference value of both the *dq* components of the VSC output current corresponding to step changes in active power reference. It can be inferred that there is again untracking and significant transient problems in the *dq* axis components of the line current while the step changes happen.

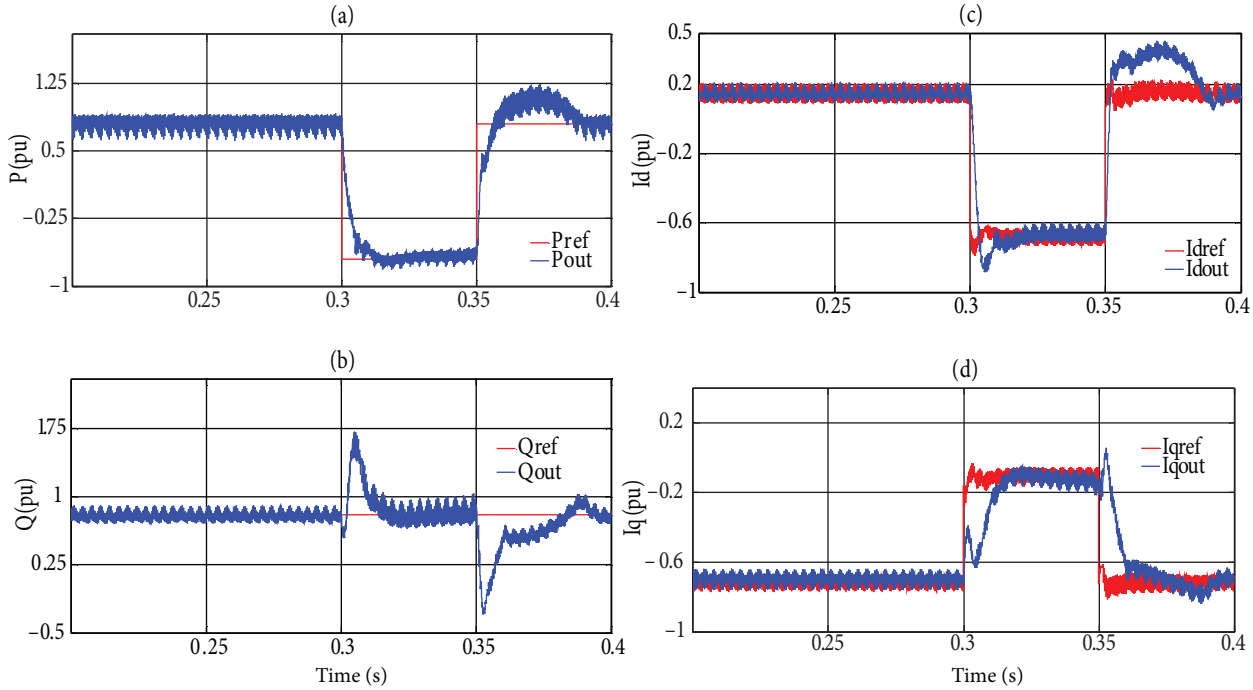

Figure 7. Transient response of the conventional controller-based power control strategy during step changes in the active power: (a) active power, (b) reactive power, (c) *d* component of the current, (d) *q* component of the current.

To evaluate the performance of the multivariable PI controller, it has been considered where the active and reactive power injected by the VSC to the grid are fixed at 0.8 p.u. At t = 0.3 s the active power steps

down to –0.7 p.u. and at t = 0.35 s it comes back to the previous value while the reactive power value is the same. Figures 8a and 8b show that after step changes in the active power reference the output active power of the VSC is rapidly regulated at the desired level with almost zero steady-state error. It is clearly specified that, contrary to the conventional power control strategy, the reactive power of the VSC experiences much less transient effect and better reference tracking due to step changes in the active power. It also imposes more decoupling properties between two kinds of power. According to Figures 8c and 8d it can be concluded that there is much less transient and better tracking in the *dq* axis components of the line current due to step changes in the active power reference.

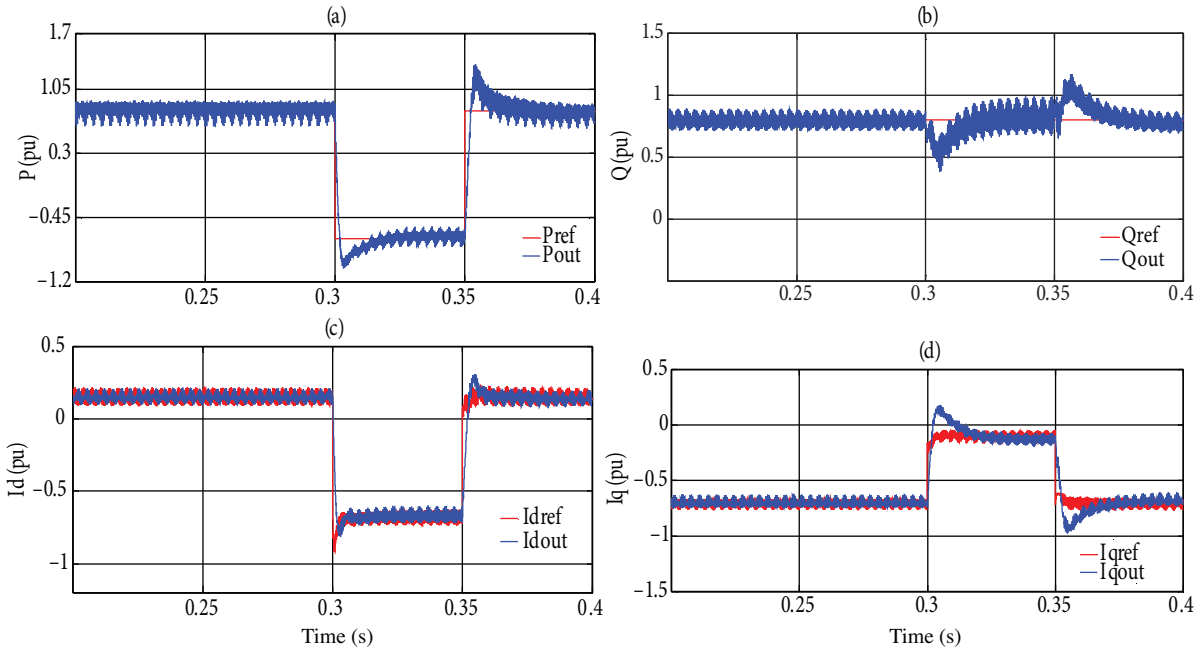

Figure 8. Transient response of the multivariable controller-based power control strategy during step changes in the active power: (a) active power, (b) reactive power, (c) *d* component of the current, (d) *q* component of the current.

A similar test is carried out to evaluate the performance of the two represented power control strategies during the step changes in the reactive power reference while the active power is kept constant. It has been considered where the active and reactive power injected by the VSC into the grid is 0.8 p.u. At t = 0.3 s the value of the reactive power steps down to –0.7 p.u. and at t = 0.35 s it steps up to the previous value. In the whole of this process, the active power value is fixed at 0.8 p.u. Figures 9a and 9b show that the output reactive power tracks its reference with almost zero steady-state error. It is clear that due to step changes in the reactive power the output active power undergoes significant effects while its reference is kept constant. This indicates the inability of the conventional power control strategy to fully decouple the powers. They also do not track their reference value well. Figures 9c and 9d show the changes in values of both the *d* and *q* axes component of the VSC output current corresponding to changes in the reactive power reference. It is shown that the *dq* components of the VSC output current have a severe transient during this process.

To analyze the response of the multivariable controller when the reactive power reference changes, it has been considered where the active and reactive power exchanged between the VSC and the grid are fixed at 0.8 p.u. At t = 0.3 s the reactive power steps down to –0.7 p.u. and at t = 0.35 s it sets back up to 0.8 p.u again. Figures 10a and 10b illustrate that after change in the reactive power reference the output reactive

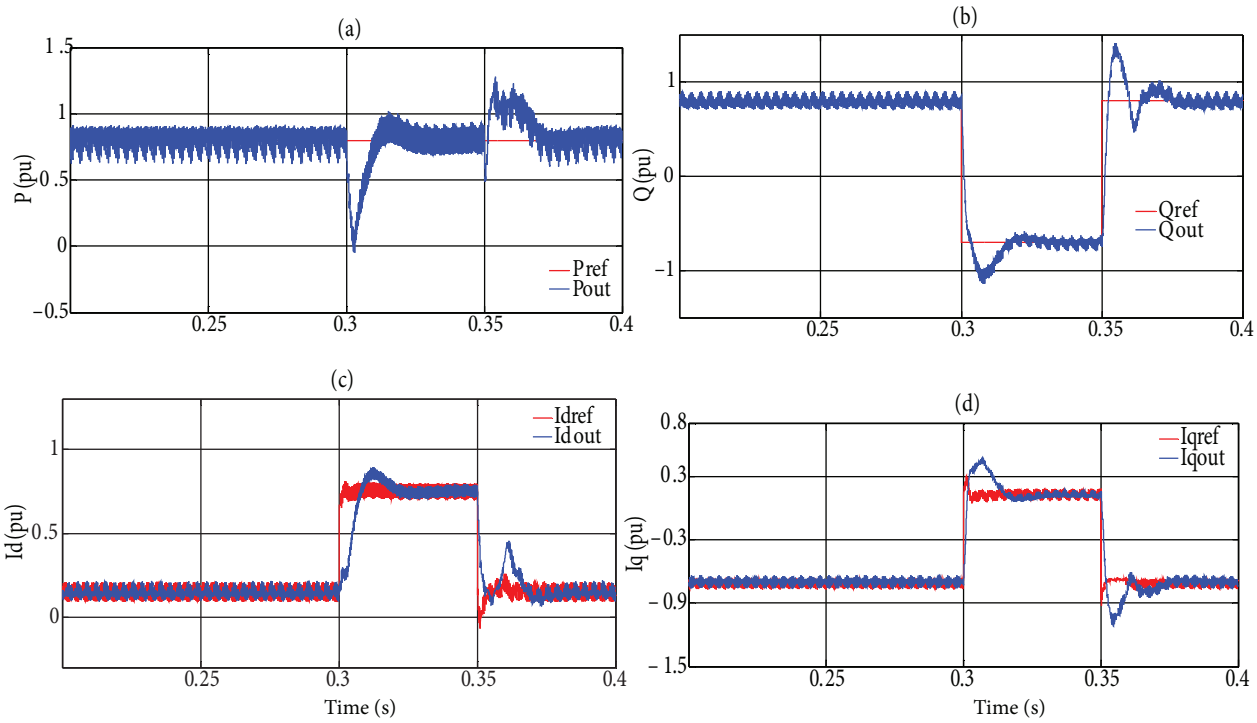

Figure 9. Transient response of the conventional controller-based power control strategy during step changes in the reactive power: (a) active power, (b) reactive power, (c) d component of the current, (d) q component of the current.

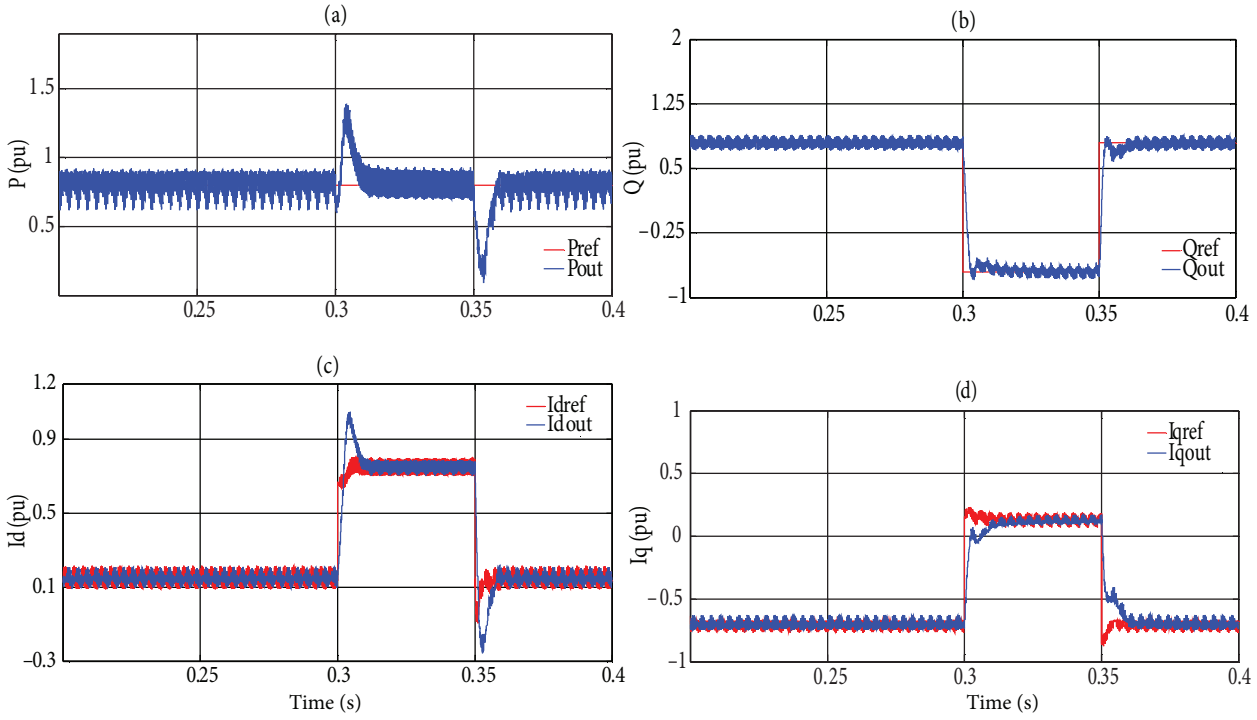

Figure 10. Transient response of the multivariable controller-based power control strategy during step changes in the reactive power: (a) active power, (b) reactive power, (c) d component of the current, (d) q component of the current.

power is rapidly regulated at the desired value with almost zero steady-state error. It is clearly specified that, compared to the conventional controller, the active power of the VSC experiences much less transient and much better reference tracking after the step changes have happened. This implies the superior decoupling capability imposed by the multivariable PI based controller. Figures 10c and 10d also depict the variation of the *dq* current components and their reference values corresponding to step changing in the reactive power. It can be concluded that there is much less transient and better tracking of the *dq* axis components of the line current during this interval.

6. Robustness evaluation with uncertainties of load parameters

This section examines the performance of the two proposed controllers with uncertainties of the load parameters in two different conditions. In each case, while the power references are changed by the utility suddenly, one load variation is imposed on the grid. After that, the power reference steps back to the initial value to evaluate the applicability of the proposed control strategy in the new situation of supplying the load. Two inductive and capacitive load changes have been investigated. Changing of the load value has occurred at time instant t = 0.35 s and after it the load contains a new condition. It has been considered in each case where the load changes abruptly occur when the converter is operating in the worst condition of supplying the load. Therefore, the reactive power exchanged between the converter and the set of the load and grid is determined independently for both cases. In the case of capacitive load, the reactive power injected by the VSC steps up to 0.5 p.u. from –0.8 p.u. at t = 0.35 s while the active power is fixed at 0.8 p.u. The simulation results are shown in Figure 11.

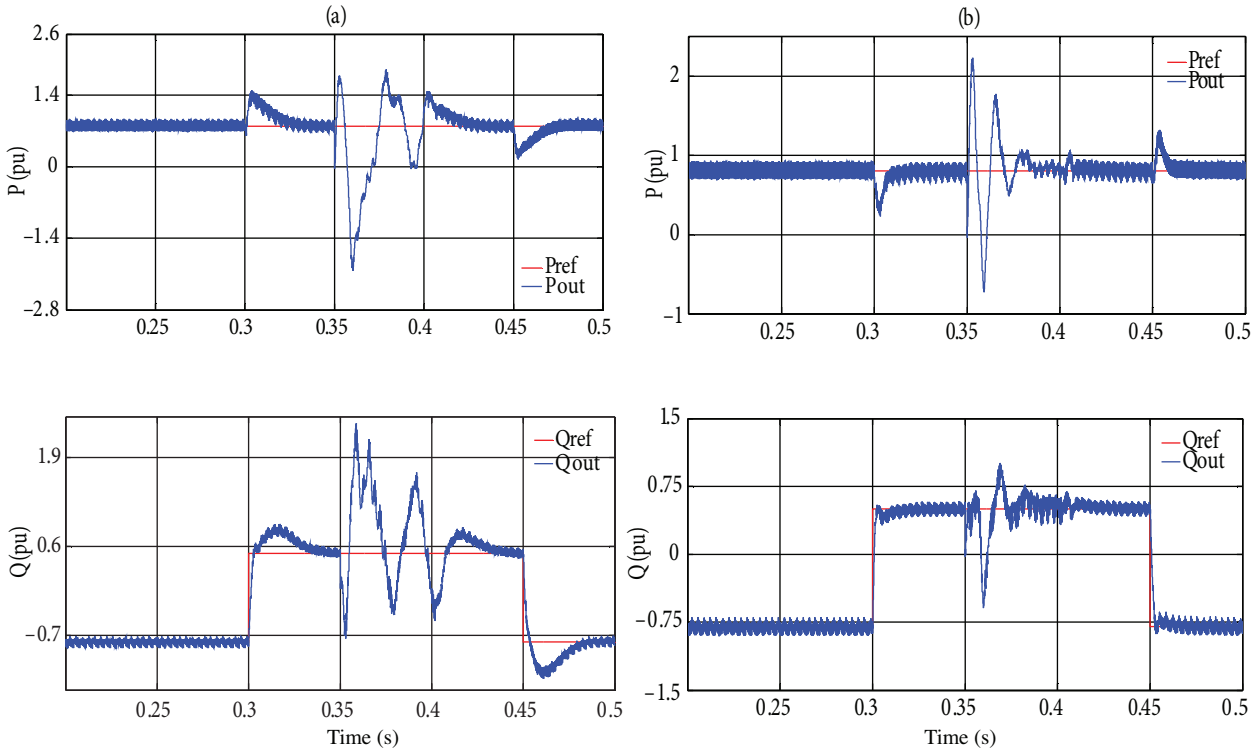

Figure 11. Dynamic response of the conventional and multivariable controller-based power control strategy with respect to changing the capacitive load: (a) conventional controller, (b) multivariable controller.

In the second case, the inductive load has been investigated. The reactive power injected by the VSC steps down to –1 p.u. from 0.8 p.u. at time instant 0.35 s while the active power is kept constant at 0.8 p.u. again. For this case, the dynamic response of two power control schemes is depicted in Figure 12. Interpreting the results at 0.35 s show that when the load changes are imposed, the system utilizing the multivariable control strategy experiences much less transient, especially in the inductive case, and moreover has better tracking of the reference values and develops the capability of more decoupled control of the active and reactive power. This is because the multivariable control strategy is not based on feedforward signals like the conventional approach. It can be concluded by investigating Figures 11 and 12 that at time instant 0.45 s the multivariable PI-based controller operates better when the reference values of the powers are set back to their previous values while the load enters into the new condition.

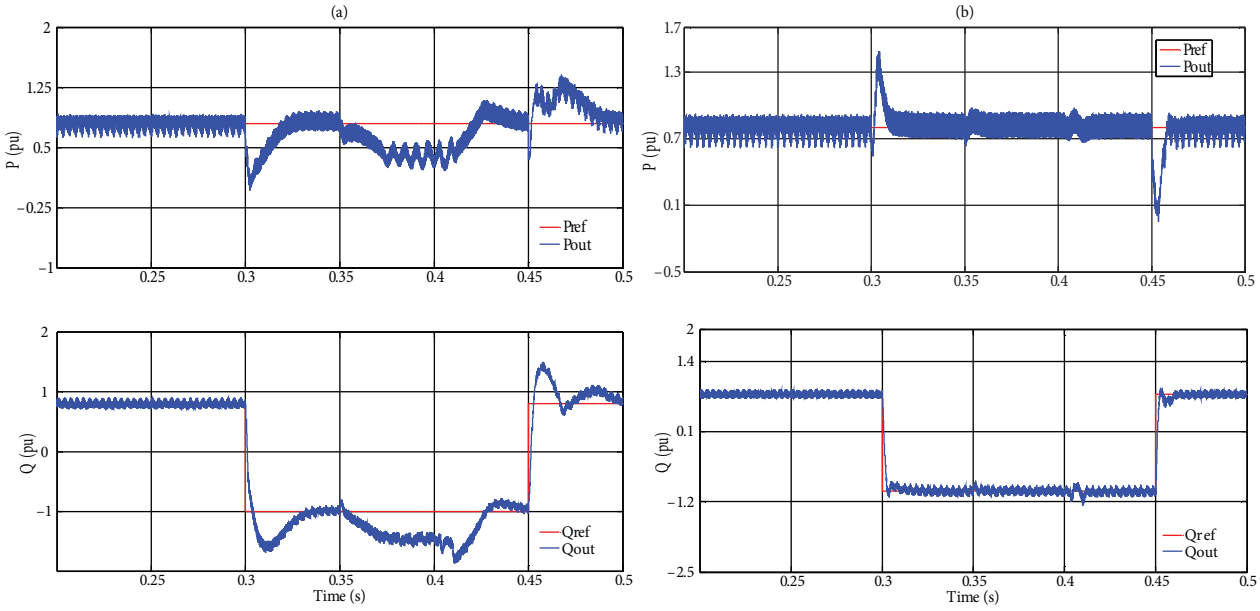

Figure 12. Dynamic response of the conventional and multivariable controller-based power control strategy with respect to changing the inductive load: (a) conventional controller, (b) multivariable controller.

7. Conclusion

In this paper, a new power control strategy has been proposed for VSC-based power conversions. Two kinds of current control strategies have been used as the inner loop of the PQ control structure and compared together to achieve better control of the output power of the VSC. The superiority of the proposed power control strategy based on the multivariable PI-controller has been evaluated in different situations of supplying the load. The superiority of the multivariable controller-based power control strategy in tracking the power reference values with almost zero steady-state error during the step changes at the load has been represented. It has also been demonstrated that the proposed power control strategy provides fast dynamics and less transient effect in the active and reactive output power than the conventional approach and has the capability of more decoupled control of the active and reactive power. The performance of the proposed control strategy in rejecting imported disturbances that occur due to uncertainties of the load parameters has also been investigated. It has been depicted that the multivariable-based power control strategy response is much better at the time instant of the load variation, having superior operation while the reactive power references come back to their initial values and the load enters the new condition.

References

[1] Singh B, Sharma S. Design and implementation of four leg voltage source converter-based VFC for autonomous wind energy conversion system. IEEE T Ind Electron 2012; 59: 4694–4703.

[2] Torres-Olguin RE, Molinas M, Undeland T. Offshore wind farm grid integration by VSC technology with LCC-based HVDC transmission. IEEE T Sus Energy 2012; 3: 899–907.

[3] Gomis-Bellmunt O, Junyent-Ferre A, Sumper A, Bergas-Jane J. Control of a wind farm based on synchronous generators with a central HVDC-VSC converter. IEEE T Power Sys 2011; 26: 1632–1640.

[4] Byon E, Perez E, Ding Y. Simulation of wind farm operations and maintenance using discrete event system specification. T Soc Model Simul I 2010; 87: 1093–1117.

[5] Abbes M, Belhadj J, Ben Abdelghani Bennani A. Design and control of a direct drive wind turbine equipped with multilevel converters. Renew Energ 2010; 35: 936–945.

[6] Choi W, Lai J. High efficiency grid connected photovoltaic module integrated converter system with high speed communication interfaces for small scale distribution power generation. Sol Energy 2010; 84: 636–649.

[7] Wasynczuk O, Anwah NA. Modeling and dynamic performance of a self-commutated photovoltaic inverter system. IEEE T Energy Conver 1989; 4: 322–328.

[8] Shimizu T, Hashimoto O, Kimura G. A novel high performance utility interactive photovoltaic inverter system. IEEE T Power Electr 2003; 18: 704–711.

[9] Mohr M, Franke WT, Wittig B, Fuchs FW. Converter systems for fuel cells in the medium power range a comparative study. IEEE T Ind Electron 2010; 57: 2024–2032.

[10] Jovcic D, Lamont L, Abbott K. Control system design for VSC transmission. Elect Pow Sys Res 2007; 77: 721–729.

[11] Fung R, Yang R. Application of VSC in position control of a nonlinear electrohydraulic servo system. Comput Struct 1998; 66: 365–372.

[12] Latorre HF, Ghandhari M, Söder L. Active and reactive power control of a VSC-HVDC. Elect Pow Sys Res 2008; 78: 1756–1763.

[13] Hu J, Yuan X. VSC-based direct torque and reactive power control of doubly fed induction generator. Renew Energ 2012; 40: 13–23.

[14] Etxeberria-Otadui I, Viscarret U, Caballero M, Rufer A, Bacha S. New optimized PWM VSC control structures and strategies under unbalanced voltage transients. IEEE T Ind Electron 2007; 54: 2902–2914.

[15] Gao F, Iravani MR. A control strategy for a distributed generation unit in grid connected and autonomous modes of operation. IEEE T Power Deliver 2008; 23: 850–859.

[16] Wang Y, Lu Z, Min Y. Analysis and comparison on the control strategies of multiple voltage source converters in autonomous microgrid. In: 10th IET International Conference on Developments in Power System Protection, 2010. pp. 1–5.

[17] Liserre M, Teodorescu R, Blaabjerg F. Multiple harmonics control for three phase grid converter systems with the use of PI-RES current controller in a rotating frame. IEEE T Ind Electron 2006; 21: 836–841.

[18] Jung J, Choi Y, Leu VQ, Choi HH. Fuzzy PI-type current controllers for permanent magnet synchronous motors. IET Electr Power App 2011; 5: 143–152.

[19] Kazmierkowski MP, Malesani L. Current control techniques for three phase voltage source PWM converters: a survey. IEEE T Ind Electron 1998; 45: 691–703.

[20] Lee TS, Tzeng KS. Input output linearizing control with load estimator for three phase AC/DC voltage source converters. In: 33rd Power Electronics Specialists Conference, 2002. pp. 791–795.

[21] Nikkhajoei H, Iravani R. Dynamic model and control of AC/DC/AC voltage sourced converter system for distributed resources. IEEE T Power Deliver 2007; 22: 1169–1178.

[22] Mohd A, Ortjohann E, Morton D, Omari O. Review of control techniques for inverters parallel operation. Elect Pow Sys Res 2010; 80: 1477–1487.

[23] Guo XQ, Wu WY, Rong Gu H. Modeling and simulation of direct output current control for LCL-interfaced grid connected inverters with parallel passive damping. Simul Model Pract Th 2010; 18: 946–956.

[24] Bahrani B, Kenzelmann S, Rufer A. Multivariable PI-based dq current control of voltage source converters with superior axis decoupling capability. IEEE T Ind Electron 2011; 58: 3016–3068.

[25] Reyes M, Rodriguez P, Vazquez S, Luna A, Teodorescu R, Carrasco JM. Enhanced decoupled double synchronous reference frame current controller for unbalanced grid voltage conditions. IEEE T Power Electr 2012; 27: 3934–3943.

[26] De Brabandere K, Bolsens B, Van den Keybus J, Woyte A, Driesen J, Belmans R. A voltage and frequency droop control method for parallel inverters. IEEE T Power Electr 2007; 22: 1107–1115.

[27] Wei LY, Kao CN. An accurate power control strategy for power electronics-Interfaced distributed generation units operating in a low voltage multi bus microgrid. IEEE T Power Electr 2009: 24: 2977–2988.

[28] Guerrero JM, Matas J, Garcia de Vicuna L, Castilla M, Miret J. Decentralized control for parallel operation of distributed generation inverters using resistive output impedance. IEEE T Ind Electron 2007; 54: 994–1004.

[29] Vasquez JC, Guerrero JM, Luna A, Rodriguez P, Teodorescu R. Adaptive droop control applied to voltage source inverters operating in grid connected and islanded mode. IEEE T Ind Electron 2009; 56: 4088–4096.

[30] Rufer A, Bahrani B, Kenzelmann S, Lopes L. Vector control of single phase voltage source converters based on fictive axis emulation. In: IEEE Energy Conversion Congress and Exposition, 2009. pp. 2689–2695.

[31] Schauder S, Mehta H. Vector analysis and control of advanced static VAR compensators. IEE P-Gener Transm D 1993; 140: 299–306.

[32] Bühler H. Réglage des Systèmes d'Électronique de Puissance. Lausanne, Switzerland: PPUR Presses Polytechniques et Universitaires Romandes, 1997.